



Article

Performance of High-Strength Concrete with the Effects of Seashell Powder as Binder Replacement and Waste Glass Powder as Fine Aggregate

Prathibha P. Shetty ¹, Asha U. Rao ^{1,*}, B. H. V. Pai ¹ and Muralidhar V. Kamath ²

¹ Department of Civil Engineering, Manipal Institute of Technology, Manipal Academy of Higher Education, Manipal 576104, Karnataka, India

² Apple Chemie India Private Limited, Nagpur 441108, Maharashtra, India

* Correspondence: asha.prabhu@manipal.edu

Abstract: Seashell powder (SSP) is a waste from aquatic life that is generally available near the coastal region. Due to its high calcium content, SSP can be utilized as a supplementary cementitious binder. SSP can be used as a sustainable binder to replace ordinary Portland cement (OPC) and significantly reduce the carbon footprint. The present study investigates the effects of SSP and waste glass powder (WGP) on the fresh, mechanical, and microstructure properties of high-strength concrete (HSC). The SSP utilized in this research was varied, with 5%, 10%, and 15% cement replacement levels. The impact of WGP was also observed with two replacement levels, 5% and 10%, replacing natural sand. The slump flow of all the HSC mixes varied between 700 and 785 mm. A maximum compressive strength of 112.91 MPa was found for the C75SSP5 mix at 56 days. The split tensile strength values of all the HSC mixes were found in a range from 5.45 to 10.56 MPa. The modulus of elasticity values of all the HSC mixes were found to lie between 40.2 and 46.8 GPa. The lowest water absorption was observed in the mix containing 5% SSP. The SEM image of the HSC with increased SSP showed that it was denser and had fewer unreacted particles. XRD and EDS showed the presence of various gels, such as calcium silicate hydrates (CSHs), ettringite, calcium hydroxide (CH), and calcium carbonate (CC). The predicted equations for its split tensile strength, flexural strength, modulus of elasticity, and water absorption were also carried out in the present research.

Keywords: compressive strength; high-strength concrete (HSC); seashell powder (SSP); waste glass powder (WGP); water absorption



Citation: Shetty, P.P.; Rao, A.U.; Pai, B.H.V.; Kamath, M.V. Performance of High-Strength Concrete with the Effects of Seashell Powder as Binder Replacement and Waste Glass Powder as Fine Aggregate. *J. Compos. Sci.* **2023**, *7*, 92. <https://doi.org/10.3390/jcs7030092>

Academic Editor:
Francesco Tornabene

Received: 3 January 2023
Revised: 21 January 2023
Accepted: 1 February 2023
Published: 2 March 2023



Copyright: © 2023 by the authors. Licensee MDPI, Basel, Switzerland. This article is an open access article distributed under the terms and conditions of the Creative Commons Attribution (CC BY) license (<https://creativecommons.org/licenses/by/4.0/>).

1. Introduction

Due to rapid developments in high-rise buildings and infrastructure advancements across the globe, there are numerous applications of HSC in the construction industry [1–4]. Significant changes have taken place in the properties of concrete and its constituents in the past 50 years. Concrete is a useful material that can easily be mixed to meet a variety of special needs and molded to essentially any shape. At present, concrete is in high demand, especially in developing countries. This demand can be met by generating cost-effective concrete by using its substitutes to enhance certain qualities and reduce its impact on the environment. The early deterioration of normal concrete structures in aggressive environments has led to the need for HSC. Harmful substances such as chloride, sulphate ions, and carbon dioxide in water and also in oxygen, which penetrate into the concrete, are liable to cause reductions in concrete strength. This problem can be solved by incorporating mineral admixtures as partial replacements for cement. Improvements in the density of the pore structure check the ingress of harmful materials into the concrete, thereby improving its strength and durability.

Compared with normal-strength concrete, HSC possesses very high strength. HSC has very low permeability, with increased resistance to corrosion in severe environments. An

experiment conducted using cementitious materials showed that they have less permeability than normal concrete. The permeability of HSC with cementitious materials is 100 times higher than that of normal conventional concrete [5–8]. In civil engineering, HSC has a wide range of applications because of its increased strength. It is used in bridges to reduce the number of beams needed to support the slab. It is highly recommended in hydropower structures due to its performance in handling the high speed of water and huge amounts of silt. The early strength gain of HSC, its low permeability, and its improved abrasion resistance are the key points which have led to HSC being used in highway pavements. As HSC can be applied for service quickly, it is also used to repair damaged pavement. HSC is further used in protections from high-density radiation, bulk concrete projects, noise and vibration damping of offshore platforms, tall structures, and tunnels. Due to reductions in the dead load, vibration, deflection, and maintenance of concrete, HSC is used in high-rise buildings. Compared with normal concrete structures, fiber-reinforced HSC acts as a repair material due to its high mechanical performance. Prefabricated HSC sleepers are used in modern high-speed railway tracks for their higher stability [9,10].

With advancements in technology, there is a need for concrete of higher strength. HSC is one such class of concrete that has been formulated in recent decades owing to its exceptional properties of strength. It is widely used around the world as its performance over normal concrete is “innovative, enhanced, and upgraded”. The addition of pozzolana can increase the compressive strength to 150 MPa, which is very significant in HSC production. Obtaining HSC involves more consideration of the proper design in terms of mixing, assembling, placing, and curing the concrete. The design of a suitable concrete mixture plays an important role for determining the type of HSC materials and structures used. The stability of concrete structures depends mostly on the durability of concrete itself. HSC, with its dense microstructure and very low permeability, has more durability than ordinary concrete. The deterioration of concrete under high temperatures could be reduced to an extent by incorporating steel fiber [11–15].

The blended binders generally include OPC, silica fume (SF), slag, fly ash (FA), etc. Recent studies also tend towards using various alternative binders such as agricultural wastes, clay, ferrochrome slag, C&D wastes, etc. Calcined limestone clay cement and ferrochrome slag aggregates have been found to be ecofriendly binders with improved mechanical performance [16–24]. The present study focuses on an alternative binder material, SSP. Waste seashells comprise another possible waste material readily available to use as a binder. Oyster, mussel, scallop, periwinkle, and cockle shells are among the various waste seashells obtainable [25]. The State of World Fisheries and Aquaculture 2020 reported that 26,000 tons of seashells and bones are produced each year. Most of this proportion of seashell debris comprises oyster, clam, scallop, and mussel shells, with just a tiny proportion being reused for other applications such as fertilization and crafts [26]. Due to the limited availability of seashell powder that may be utilized as a binder and the issues of soil solidification and economic matters, reuses are minimal. Furthermore, there are challenges with waste seashells being dumped illegally into open waters and reclaimed land. If seashells remain untreated over an extended period, they can emit foul odors due to the breakdown of the leftover muscles in the shells or the microbial decomposition of salts into gases such as H_2S , NH_3 , and ammonia products. The biodegradation of seashells can significantly impact the quality of life of those living nearby and cause environmental contamination. The current study utilizes waste SSP, which reduces OPC use. The bare-minimum use of OPC can reduce greenhouse gas and CO_2 emissions, achieving sustainability goals [27–29].

In addition, WGP is another material used to replace fine aggregate. Glass is a popular material that can be found practically anywhere and in various shapes, including in food jars, decorative items, laboratory equipment, cold drink urns, tubes, lights, and monitors. India produces thousands of tons of regulated glass trash from residential, institutional, and industrial activity. It is nearly 100 percent recyclable, but with the current collection and recycling network, only 45 percent of glass is recycled. The usage of WGP reduces

the consumption of natural sand and quartz sand [30–34]. WGP has a significant effect on concrete's setting and flow properties. WGP content in concrete reduces its flow and setting. However, the mechanical properties of concrete are decreased slightly compared with concrete without WGP. Nanosized glass waste with FA in cement showed good engineering properties along with minimizing environmental hazards [35–39].

Various studies have tried to utilize many supplementary cementitious materials. The mechanical properties of HSC, such as compressive strength, split tensile strength, flexural strength, modulus of elasticity, and water absorption, with the effect on waste binders, have been studied. Yang Zhang et al. (2020) investigated utilizing concrete as a material for the durability and reinforcement of deteriorated conventional concrete structures due to its excellent characteristics, such as superior compressive strength, high tensile capacity, and extremely low permeability [40]. Ye Shi et al. (2019) have aimed to prove that concrete with high strength is used to reduce the harmful effects of building materials on the environment and post-maintenance compared with standard concrete. A study of HSC presented a series of comprehensive methods, including the optimization design of the binder system, the utilization of nanoparticles and chemical activators, and heat curing to prepare HSC with relatively lower environmental impact [41].

Xie et al. (2018) studied shrinkage's impact in concrete. Three unique practices to reduce the effect of shrinkage were investigated: reducing the powder content, chemical admixture, and using crushed ice to partly substitute mixing water [42]. Sarcomas et al. (2018) have studied the effects of constituent materials on the microstructure and mechanical properties of concrete. An attempt was made to study the rheological properties of concrete using a squeezing flow test [43]. Suleyman et al. (2017) have concentrated on producing high-strength concrete by using pumice aggregate to gain an advantage in transportation due to its low weight. Brass-coated steel fibers and polycarboxylate-based superplasticizers were utilized with OPC and silica fumes [44]. Hiremath and Yaragal (2017) have studied the effects of standard, steam (hot water bath), autoclave, and combined (steam and standard) curing regimes on the early strength development of HSC. HSC studies have revealed that steam curing was found to have the highest strength among the four different curing regimes. Seashell and mussel shell powders were used to replace OPC in the range of 5%–20%. Replacement with seashell binders increased the mechanical and microstructure properties but adversely reduced the setting and flow characteristics. The influence of curing days on the enhancement of mechanical properties at the early phases is considerably more critical than the impact of the later curing days [45–51]. The details in the literature have displayed various studies of curing regimes, materials used, methods, and different studied mechanical properties. The literature mentioned above indicates that limited research has been conducted on SSP and WGP utilization.

The current study aims to find the optimum percentages of SSP as a binder replacement and WGP as a fine aggregate replacement in HSC. This investigation focuses on the effect of SSP, which varied with 5%, 10%, and 15% cement replacement levels. In addition, the impact of WGP was observed with two replacement levels, 5% and 10%, replacing natural sand. The report also includes the fresh properties of HSC such as slump flow, T500, and T700. This research also considers mechanical properties such as the compressive strength, split tensile strength, flexural strength, modulus of elasticity, and water absorption of HSC with SSP and WGP. The microstructure of HSC was also studied using SEM, EDS, and XRD. The present investigation also includes the predicted equations for split tensile strength, flexural strength, modulus of elasticity, and water absorption.

2. Materials and Methods

2.1. Binders

Concrete is considered to be a two-phase material, consisting of the paste or cement phase and solid or aggregate phase. The overall properties of concrete are influenced by both the properties and qualities of paste phase as compared with those of aggregate phase. The properties, such as strength, elastic properties, permeability, durability, and change in

volume of concrete, are highly influenced by the concrete’s paste structure. Figure 1 shows the different binder materials used in the present study.

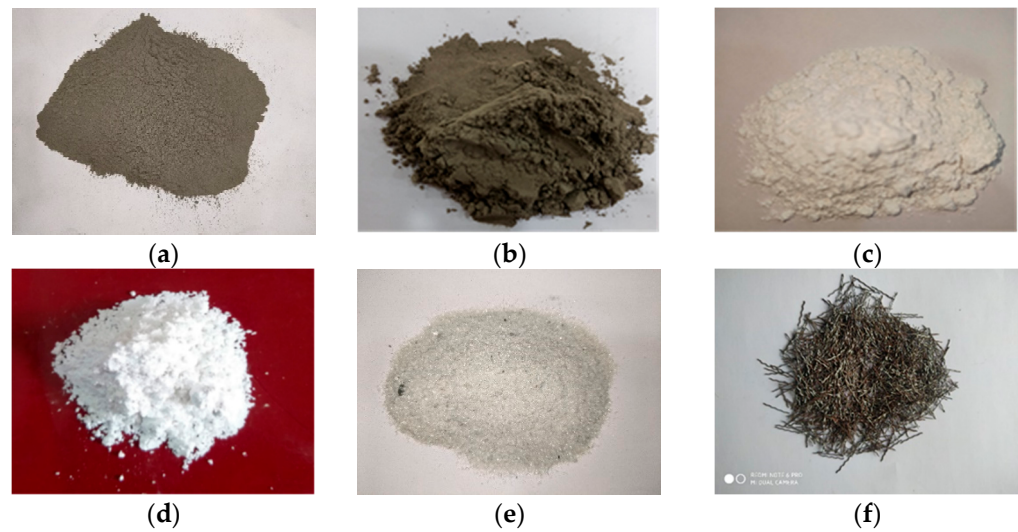


Figure 1. Materials used to develop HSC: (a) OPC 53; (b) Class C FA; (c) SF; (d) SSP; (e) WGP; (f) steel fibers.

2.1.1. OPC

OPC 53 grade conforming to IS 12269 was utilized in binder systems in the present work. The compressive strength of cement mortar as per IS 4031 should not be less than 53 MPa at 28 days. The obtained test results of OPC 53 grade are tabulated in Table 1. Ramco brand of OPC was procured from a local supplier. The specific gravity and surface area of OPC 53 were 3.10 and 240 m²/kg, respectively. The chemical and physical properties of OPC 53 grade are tabulated in Tables 2 and 3. PSD and SEM images of OPC 53 grade are shown in Figures 2 and 3a.

Table 1. Test results of OPC 53 grade.

Content	Fineness	Specific Surface m ² /kg	Normal Consistency	Specific Gravity	Setting Time		Compressive Strength (MPa)		
					Initial	Final	72 ± 1 h (3 days)	168 ± 2 h (7 days)	672 ± 4 h (28 days)
Requirement as per IS:12269-1987	225 (min)		25–35%	3.15	30 min	600 min	33 (min)	43 (min)	53 (min)
Test Results	240		30%	3.1	40	211	37.54	45.71	54.82

Table 2. Physical properties of powder materials.

Physical Characteris- tics		OPC 53	Class C FA	SF	SSP
Specific Gravity		3.10	2.65	2.35	2.62
Specific Surface Area (m ² /kg)		240	446	23,500	1988
Particle Size	d10	3.70 (µm)	2.91 (µm)	1.11 (µm)	2.11 (µm)
	d50	14.83 (µm)	15.68 (µm)	3.67 (µm)	5.88 (µm)
	d90	32.20 (µm)	70.94 (µm)	8.26 (µm)	15.77 (µm)

Table 3. Chemical properties of powder materials.

Chemical Component	OPC 53	Class C FA	SF	SSP
CaO	58.66	16.1	1.2	47.49
SiO ₂	21.27	34.8	91	
Al ₂ O ₃	8.79	14.1	2.4	
Fe ₂ O ₃	3.56	24.14		
MgO	1.94	2.7	1.28	0.619
K ₂ O	-	1.3		
Na ₂ O	-	5.3		1.119
SO ₃	2.52	0.5	0.64	0.403
TiO ₂	1.35	0.86		
LOI	1.48	2.64	2.08	

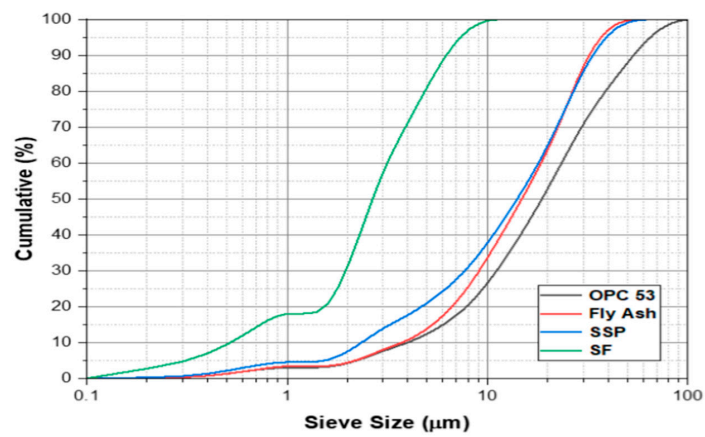


Figure 2. Particle size distribution of powder binder materials.

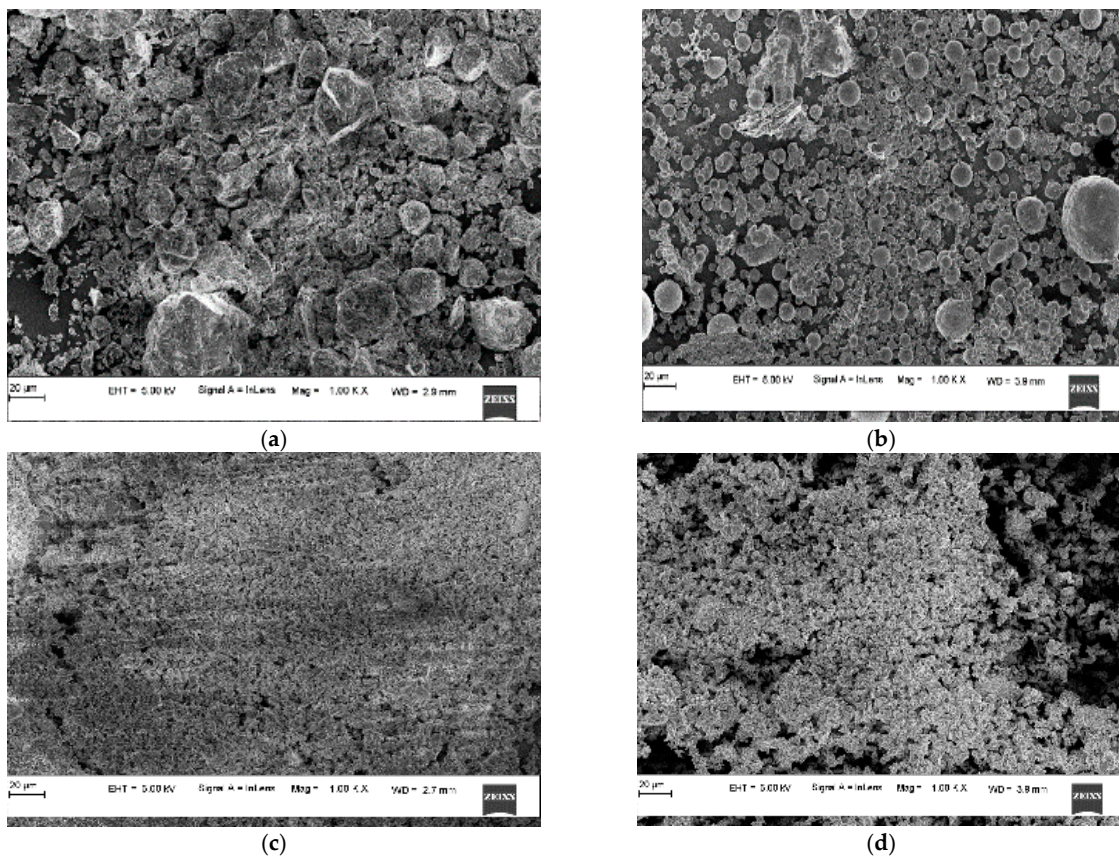


Figure 3. SEM images of powder materials: (a) OPC 53; (b) class C FA; (c) SF; (d) SSP.

2.1.2. Silica Fume

SF is also known as microsilica, produced from silicon metal and other ferrosilicon alloys. In the present study, SF was used in HSC owing to its high reactivity and fineness. SF fulfilled the criteria as per ASTM C 1240. The specific gravity and surface area of SF were 2.35 and 23,500 m²/kg, respectively. The chemical and physical properties of SF are presented in Tables 2 and 3. SF was procured from Astra Chemical Limited, Chennai, India. PSD and SEM images of SF are shown in Figures 2 and 3b.

2.1.3. Class C Fly Ash

Class C FA was collected from an RTPS, Raichur, India. Class C FA satisfied the chemical composition requirement criteria as per clause of ASTM C618. The specific gravity and surface area of FA were 2.65 and 446 m²/kg, respectively. The chemical and physical properties of Class C FA are presented in Tables 2 and 3. PSD and SEM images of Class C FA are shown in Figures 2 and 3c.

2.1.4. Seashell Powder

SSP is a composite binder containing more than 90% calcium carbonate by its weight. SSP is produced by grinding the oyster shells found in the marine ecosystem and calcining them at 600 to 700 °C. The chemical and physical properties of SSP are presented in Tables 2 and 3, respectively. Calcium-rich SSP has shown promising results in a few studies. PSD and SEM images of SSP are shown in Figures 2 and 3d.

2.2. Fine Aggregate

2.2.1. Natural Sand

Natural sand was procured from a local supplier. The sand used in the mix was made to pass through a 2.36 mm IS sieve, and its water absorption was found to be less than 2% with specific gravity of 2.61.

2.2.2. Waste Glass Powder

WGP left over after cutting glasses was collected from local glass manufacture shops. WGP materials cannot be reused because of the high cost of recycling. WGP was grounded to below 150 microns and was used as a partial replacement for cement and fine aggregate. XRD of WGP and SSP is shown in Figure 4. WGP was in amorphous phase and SSP was in crystalline phase with CaO as the major peak as compared with Ca(OH)₂ and CaCO₃.

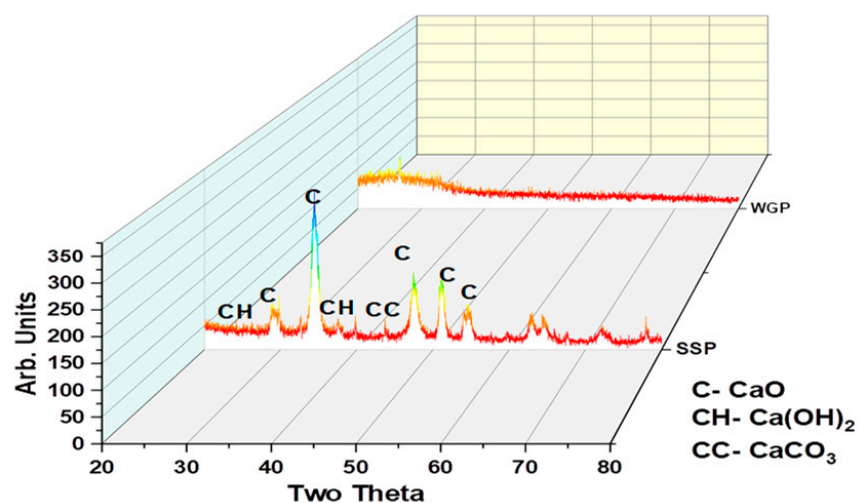


Figure 4. XRD of SSP and WGP.

2.3. Chemical Admixture

Polycarboxylate-ether-based (PCBE) superplasticizer Mapei Dynamon 550 was used for its high workability and to achieve high mechanical properties of HSC. The use of PCBE reduced the w/c ratio to 0.20 for a dosage of less than 2%.

2.4. Steel Fibers

The steel fibers used were 12.5 mm long and 0.45 mm in diameter, and the fibers were in a crimped shape. The density of steel fibers was 7850 kg/m³ and the fibers were corrosion-free. The characteristics of steel fibers are tabulated in Table 4.

Table 4. Characteristics of steel fibers.

Material	Shape	Length (mm)	Diameter (mm)	Aspect Ratio	Tensile Strength (MPa)	Density (kg/m ³)
Stainless steel	Corrugated	12.5	0.45	27.7	1100	7850

2.5. Mix Proportions

Mixes of concrete with high strength published by various authors were referred to and adopted in the present work [13,51]. HSC mixes were then developed using a trial-and-error procedure. Mix proportions were achieved based on trial and error, and the number of materials used to prepare the various mixes of HSC is tabulated in Table 5. C90SSP0 and C80SSP0 are referred to as reference mixes; details are given in Table 5. The effect of SSP in HSC was studied with 5%, 10%, and 15% cement replacement levels. The impact of WGP was also examined with replacement of natural sand in two groups at 5% and 10%. The total binder content of 1000 kg/m³ was constant throughout all mixes. The w/c ratio of 0.2 was kept constant in the present study. PCBE superplasticizer was fixed at 2% binder content throughout the blends. In addition, steel fibers used were observed at 3% of the total volume in all mixes. Various mechanical properties of seven different HSC mixes were studied.

Table 5. Mix proportions for HSC.

Mix Designation	OPC (%)	SF (%)	FA (%)	SSP (%)	Quartz Sand(kg/m ³)	WGP (%)	Superplasticizer (%)	Water to Cement Ratio	Steel Fibers (% by Weight)
C90SSP0	90	10	-	-	877	-	0.15	0.20	3
C80SSP0	80	10	10	-	877	-	0.15	0.20	3
C75SSP5	75	10	10	5	877	-	0.15	0.20	3
C70SSP10	70	10	10	10	877	-	0.15	0.20	3
C65SSP15	65	10	10	15	877	-	0.15	0.20	3
C75SSP5GP5	75	10	10	5	827	5	0.15	0.20	3
C75SSP5GP10	75	10	10	5	777	10	0.15	0.20	3

2.6. Test Methods

A slump flow test was conducted on fresh HSC mixes to obtain a good combination as per IS:1199-1959. HSC's compressive strength was tested as per IS:516-1959 at 7, 28, and 56 days of water curing period. HSC cylinders were cast to test the splitting tensile strength of concrete specimens as per IS:5816-1999. HSC cylinders were tested after water curing for 28 and 56 days. The flexural strength of beams of size 100 × 100 × 500 mm (B × H × L), cast as per IS:516-1959, was tested at 28 and 56 days of water curing. Water absorption test was conducted on HSC samples as per codal provisions of BS 1881(122-1983). SEM-EDS and XRD were performed for microstructure properties of HSC using EVO MA18 with Oxford EDS (X-act) and Rigaku Miniflex 600.

3. Results and Discussion

3.1. Effects of SSP and WGP on Slump Flow of HSC

The slump flow of all the HSC mixes varied from 700 to 785 mm. The slump flow time for the HSC to reach a diameter of 500 mm for all the mixes was less than 8 s, and

the time needed to achieve a flow diameter of 700 mm for all mixes ranged between 20 and 25 s. The slump flow values, T500 and T700, agreed with European guidelines and are plotted in Figure 5. The C65SSP15 mix displayed the lowest slump flow value and T500, which were 738 mm and 8 sec, respectively, which may have been due to an increase in the surface area of the binder. The increased surface area led to more water being utilized by the seashell powder, significantly reducing the slump flow and slump time. Similar observations were also noted in previously published outcomes [48,49]. In addition, the increase in waste glass powder reduces the slump flow and slump time, which can be seen in the mixes C75SSP5GP5 and C75SSP5GP10.

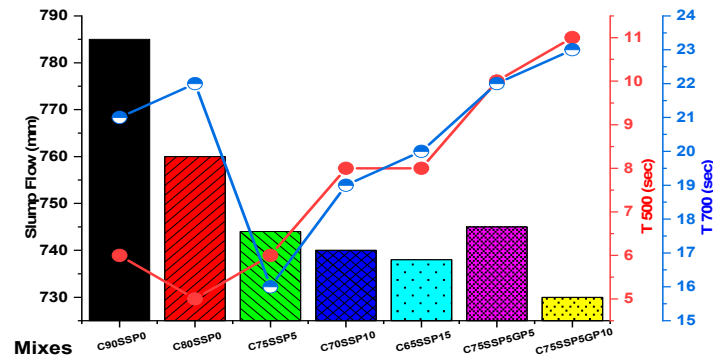


Figure 5. Slump flow, T500, and T700 of HSC mixes.

3.2. Effects of SSP and WGP on Compressive Strength of HSC Mixes

The compressive strength of various HSC mixes at 7, 28, and 56 days of underwater curing was examined, as shown in Figure 6. The HSC specimens were tested after being removed from the water and patted dry. A maximum compressive strength of 112.91 MPa was found for the C75SSP5 mix at 56 days.

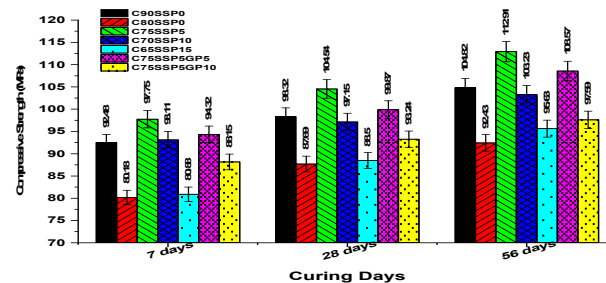


Figure 6. Compressive strength of HSC mixes.

The C75SSP5 and C75SSP5GP5 mixes showed higher strength than all five other mixes because of their additional hydrated products and higher particle packing. The C80SSP0 mix showed a slower hydration process because of its 10% FA content. The C70SSP10 and C65SSP15 mixes indicated a loss of strength as the SSP percentage increased from 5% to 15% due to the increase in CSH gel, which can be seen in the XRD and SEM images. C75SSP5GP10 showed a more significant reduction in strength than C75SSP5GP5 because its WGP content was increased from 5% to 10%. A mix containing 5% SSP and 5% GP exhibited the maximum compressive strength of the C75SSP5 and C75SSP5GP5 mixes, indicating optimum SSP and WGP. The C75SSP5 mix was also steam cured for three days at 90 °C, and compressive strength was achieved at about 154 MPa. With the inclusion of SSP, it can be noted that the compressive strength improved quickly in the early curing days; later, the compressive strength was enhanced more slowly. It can be observed that the impact of the curing days on the enhancement in compressive strength was considerably more noticeable in the early curing days compared with the later curing days, and these outcomes are in good agreement with the results displayed. Comparable results have been observed in previous findings [52–54].

3.3. Effects of SSP and WGP on Split Tensile Strength

The split tensile strength values of all HSC mixes were in the range of 5.45–10.56 MPa, as shown in Figure 7. HSC mixes showed higher strength due to the presence of 3% of the total volume of steel fibers. The C75SSP5 and C70SSP10 mixes revealed 23% and 18.37% respective increases in splitting tensile strength compared with the C90SSP0 blend, due to the strong influence of SSP reactivity and enhanced interlocking of particles with aggregates. C75SSP5GP5 indicated a 13.8% increase in splitting tensile strength compared with the C90SSP0 mix. The compressive strength results were also similar in terms of split tensile strength values. Previously published studies of HSC mixes have shown similar outcomes [55,56].

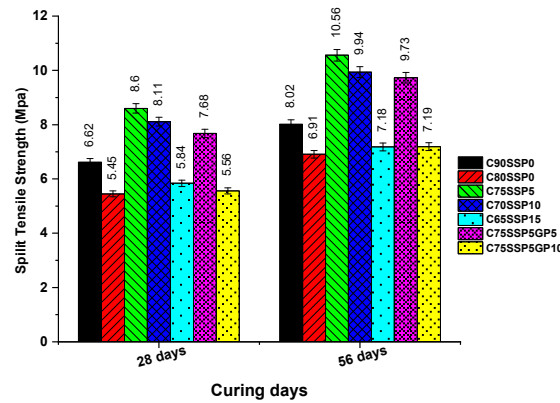


Figure 7. Split tensile strength of HSC mixes.

3.4. Effects of SSP and WGP on Modulus of Elasticity

The modulus of elasticity values of all HSC mixes were found to vary from 40.2 to 46.8 Gpa, as shown in Figure 8. The HSC mixes showed a higher modulus of elasticity due to the steel fibers. The highest modulus of elasticity value was that of the C75SSP5 mix at 46.8 GPa, and the C65SSP15 mix displayed the lowest modulus of elasticity value of 40.2 GPa. The C75SSP5 mix revealed a 4.7% increase in its modulus of elasticity compared with the C90SSP0 mix, owing to the rise in paste stiffness with 5% SSP. C75SSP5GP5 also indicated a 1.76% increase in its modulus of elasticity, because it contained 5% more WGP than the C90SSP0 mix. It can be observed that the compressive strength and split tensile strength results also indicate similar trends in terms of modulus of elasticity values. Other recent investigations of HSC mixes have yielded similar results [57–59].

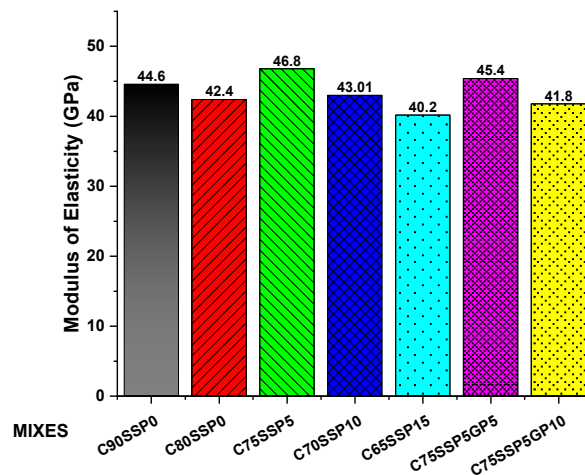


Figure 8. Modulus of elasticity values of HSC mixes at 28 days.

3.5. Effects of SSP and WGP on Water Absorption

The water absorption of all of the HSC mixes, performed at 28 days, is demonstrated in Figure 9. The water absorption reduced with increasing SSP in the mixes, and the lowest water absorption was observed in the HSC mix with 5% SSP. A combination of SSP and WGP, i.e., the C90SSP0 combination, had a water absorption value of 3.3%. The C80SSP0, C75SSP5, C70SSP10, C65SSP15, C75SSP5GP5, and C75SSP5GP10 mixes had water absorption values of 3.8, 2.9, 3.1, 3.6, 3, and 3.1%, respectively. As the percentage of SSP increased, the water absorption of the HSC mixes decreased, owing to the denser paste and lower porosity. The WGP slightly affected water absorption, which may be due to having unreacted particles and higher porosity than the C75SSP5 mix. The correlation between the water absorption and compressive strength of all of the HSC mixes was $Y = 7.80 - 0.047 \times X$, where Y is water absorption and X is compressive strength with an R2 value of 0.78. The latest studies on HSC mixes have revealed similar findings [60,61].

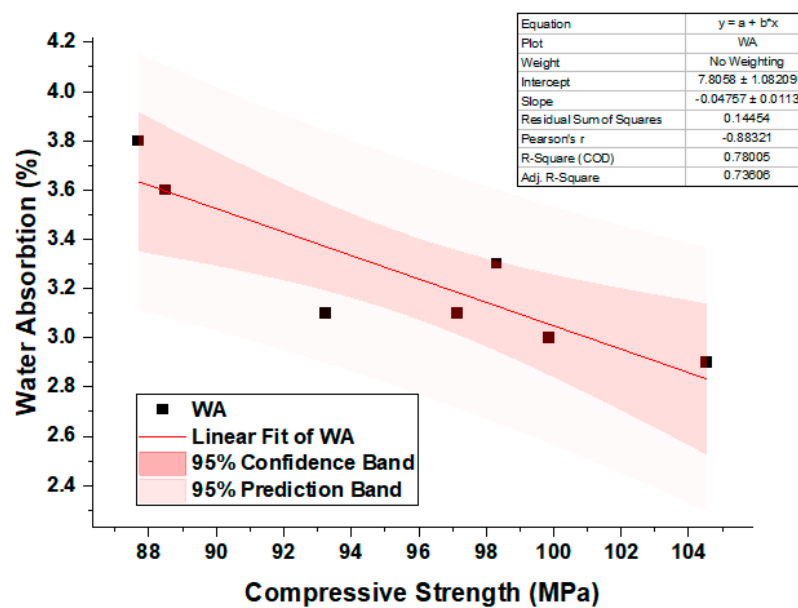


Figure 9. Water absorption of RPC combined at 28 days.

3.6. Effect of SSP in HSC Mixes Using Scanning Electron Microscope (SEM) Images

SEM analysis of the C90SSP0 mix (reference mix) is shown in Figure 10a. From the SEM micrograph of the C90SSP0 blend, it can be observed that the formation of CSH gel occurred all over the mixture in a hydrated cement paste, and that led to an increase in compressive strength with the curing time. The presence of calcium and the formation of CaCO₃ are visible in the mix, and these are the primary sources for strength gain. The C90SSP0 mix was less dense, and there was no visible ettringite formation in the combination.

SEM analysis of the C80SSP0 mix is displayed in Figure 10b. The micrographic study showed a decreased formation of CSH gel, which led to a slower hydration process. Adding 10% FA to the mix slowed the hydration process. The decrease in CSH gel was due to the presence of unreacted particles. Due to ITZ formation between the paste and the aggregate, visible cracks were found in the mix.

SEM microscopic analysis of the C75SSP5 mix is displayed in Figure 10c. The SEM images show a comparatively denser mixture, and maximum hydration was achieved at 56 days. Replacement with SSP as a binder has a considerable effect on the mechanical properties of HSC, which can be noted from the increased CSH gel formation in a hydrated paste. Nonetheless, in the C75SSP5 mix, many unreacted particles can be observed in an inactivated state; these could be further activated using heat or steam curing. Calcite formation in the combination was high, leading to strength gain. Ca and CaCO₃ increases can be seen in the mix; these are the crucial triggers for strength gain.

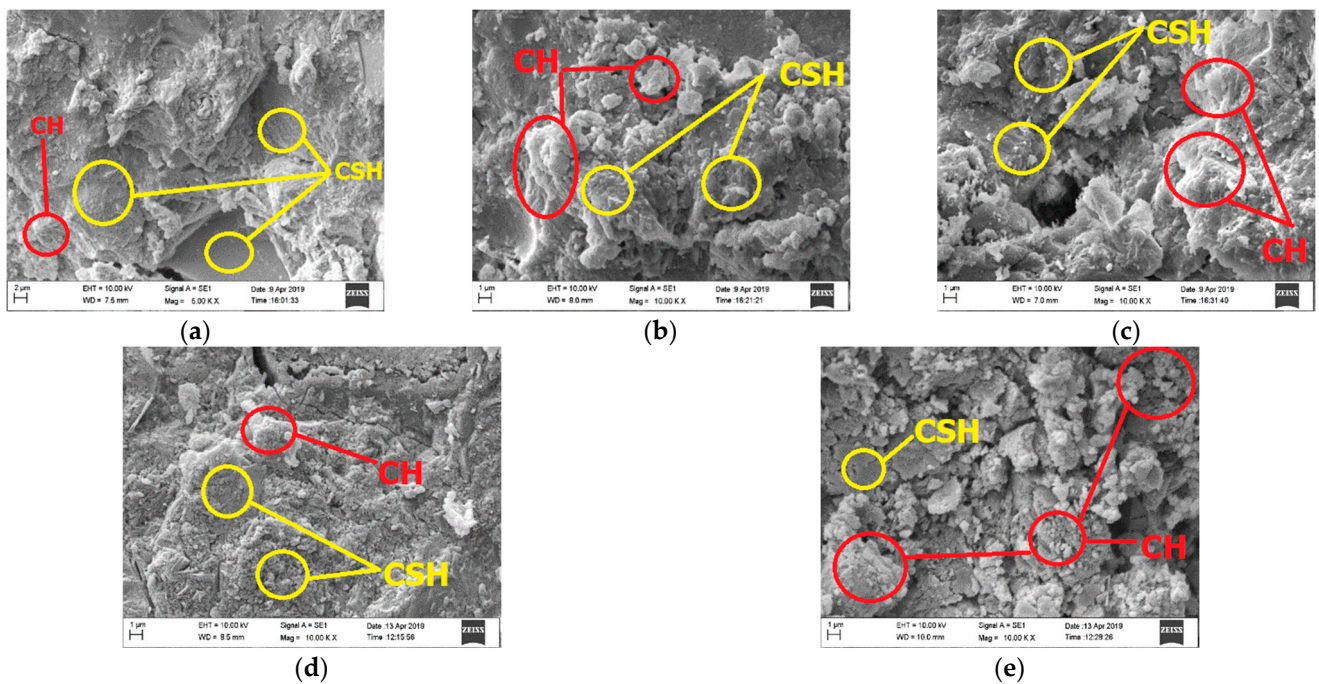


Figure 10. SEM images of all HSC mixes: (a) C90SSP0; (b) C80SSP0; (c) C75SSP5; (d) C75SSP10; (e) C75SSP15.

SEM microscopic analysis of the C70SSP10 mix is shown in Figure 10d. An increase in SSP density improved the mix density; however, ITZ development caused cracks in the mix. Increased SSP had a negative effect on the mix's mechanical performance. Increased non-hydrated elements in the mixture resulted in a loss of strength.

SEM microscopic analysis of the C65SSP15 mix is illustrated in Figure 10e. An increase in SSP led to a further decrease in CSH development due to the unreacted phase of supplementary particles. An improper bond was found between aggregate and binder particles. The CSH gel formation was inadequate, which led to a further reduction in strength. The reaction between silica content and portlandite in the mix was stopped after 28 days, which was also a possible reason for the low strength [6,12,39].

3.7. Effect of SSP on Energy-Dispersive X-ray Spectroscopy (EDS)

EDS analyses of the C90SSP0, C80SSP0, C75SSP5, C70SSP10, and C65SSP15 mixes are shown in Figure 11. EDS analysis demonstrated the presence of Ca, Si, Na, and traces of other elements in all of the HSC mixes. The Ca content in the OPC-SSP blend increased in the binders' system with an increase in SSP, which remained unreacted in the HSC mix. A substantial increment in compressive strength was found with the addition of SSP in the HSC mix. The C65SSP15 mix showed more CSH gel formation, but it was still unreacted. C75SSP5 displayed a chemically stable state compared with C70SSP10 and C65SSP15. The Ca/Si ratios of the C90SSP0, C80SSP0, C75SSP5, C70SSP10, and C65SSP15 mixes were 4.88, 4.01, 3.66, 2.45, and 2.82, respectively. According to the EDS results analysis, the development of CSH gel was prominent, and there was also the existence of CASH gel. The addition of SSP to the binder system resulted in additional CSH gel development due to the rise in calcium content. The Ca/Si ratios in the SSP-based paste decreased while the Si/Al ratios increased, contributing to the mechanical properties of the HSC mixes [56,57]. Fewer peaks of CSH formations were obtained in the XRD analysis, as shown in Figure 12.

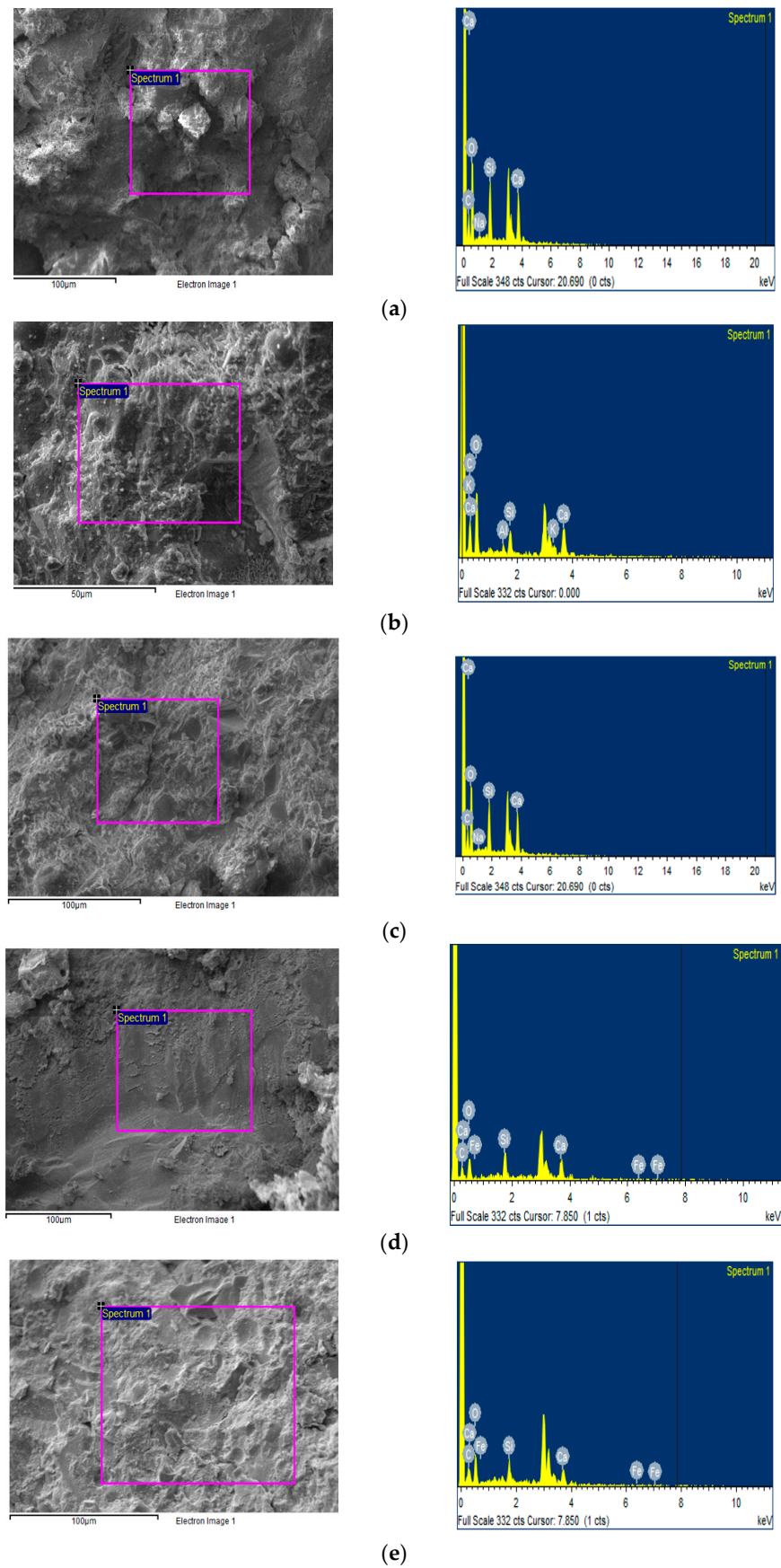


Figure 11. EDS analyses of all mixes: (a) C90SSP0; (b) C80SSP0; (c) C75SSP5; (d) C70SSP10; (e) C65SSP15.

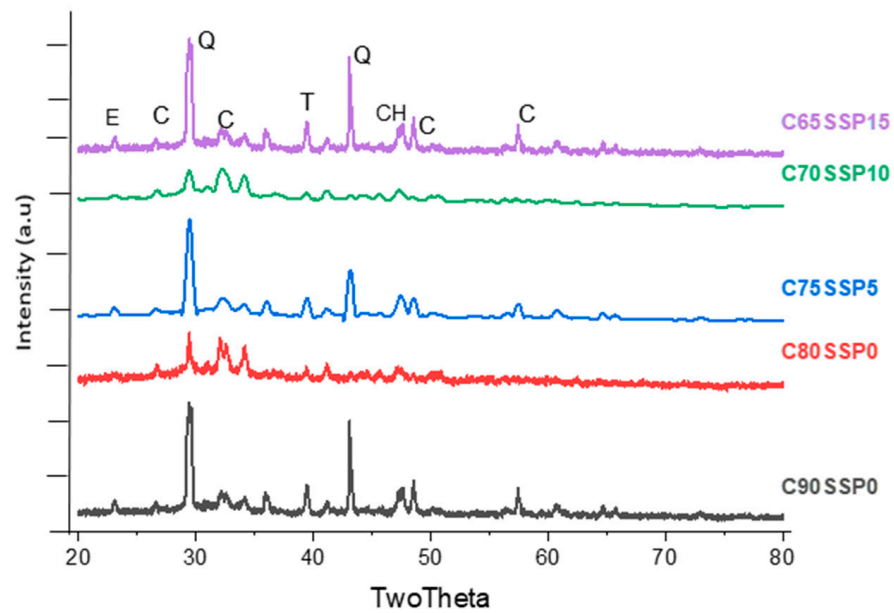


Figure 12. XRD of HSC mixes with SSP.

3.8. X-ray Diffraction (XRD)

XRD analyses of the C90SSP0, C80SSP0, C75SSP5, C70SSP10, and C65SSP15 mixes are displayed in Figure 12. The HSC mix with C75SSP5 samples exhibited higher CSH peaks than those with C70SSP10 and C65SSP15. The reaction of the SSP binder pastes indicated the new semicrystalline intensities developing in various compounds. There were few impurities from the OPC 53, SF, and FA binders in their crystalline intensities all over the binder hydration process. Since SSP is slightly more reactive compared with OPC and FA, the HSC mixes experienced complete or incomplete hydration, observing a decreased CSH peak. Ettringite was also observed with SSP and without SSP. Although SSP is more reactive than OPC and FA, the quaternary mixtures underwent a full or partial hydration process, as evidenced by the lower peak intensity of CSH. As the quantity of SSP in the quaternary mixes improved, the peak intensity of CSH increased dramatically. Since a greater SSP percentage resulted in a higher cement matrix, which added a considerable number of gels to the paste, higher SSP content resulted in more hydrates. Secondary hydrates, on the other hand, had a major impact on CH development. The cross-bonding approach increased the effectiveness of OPC, SSP, SF, and FA, resulting in a more compact binder system that greatly improved the HSC's mechanical properties. The identified peaks were Q—quartz (ICDD-01-072-0646), C—calcium silicate hydrate (ICDD-01-083-1550), E—ettringite (ICDD-01-072-0646), T—tobermorite (COD 01000046), and CH—calcium hydroxide (ICDD-01-072-0156). The XRD results are in good agreement with the SEM and EDS results.

3.9. Relationship between Mechanical Properties of HSC

3.9.1. Split Tensile Strength Versus Compressive Strength

The relationship between the split tensile strength and compressive strength of HSC at 28 days was analyzed and compared with the IS code, the ACI code, and the outcomes of Singh et al. (2022) [61], as shown in Figure 13a. The proposed equation of $Y = 0.34 \times X^{0.68}$ with an R^2 value of 0.88 was obtained using nonlinear regression analysis, where X is compressive strength (MPa) and Y is split tensile strength (MPa).

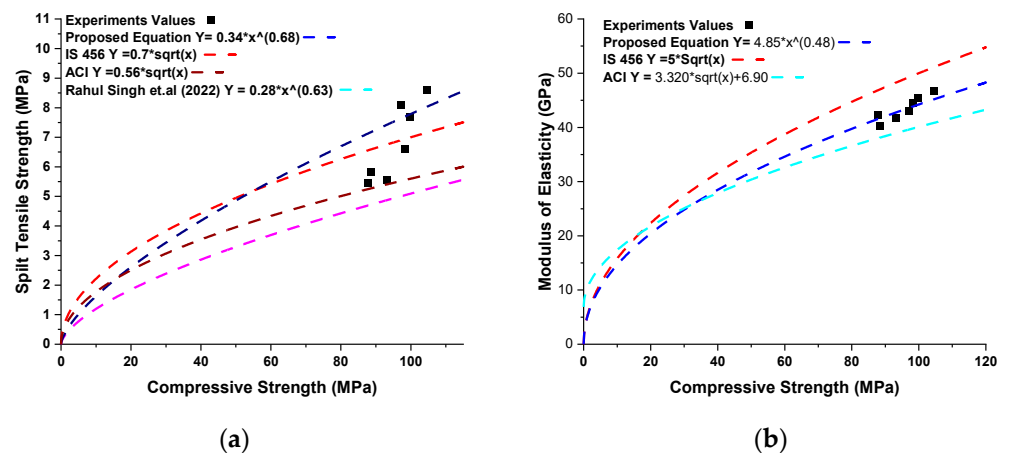


Figure 13. Relationships between mechanical properties of HSC: (a) relationship between split tensile strength and compressive strength at 28 days; (b) relationship between modulus of elasticity and compressive strength at 28 days.

3.9.2. Modulus of Elasticity Versus Compressive Strength

The relationship between the modulus of elasticity and compressive strength of HSC at 28 days was analyzed and compared with the IS code and the ACI code, as shown in Figure 13b. The predicted equation of $Y = 4.85 \times X^{(0.48)}$ with an R^2 value of 0.92 was obtained using nonlinear regression analysis, where X is compressive strength (MPa) and Y is the modulus of elasticity (GPa).

4. Conclusions

The experimental results of the effects of SSP and WGP on the fresh, mechanical, and microstructure properties of HSC are discussed below. Based on the experimental outcome, the following conclusions have been drawn:

- Seashell powder can be used as a binder that reduces OPC consumption significantly. The increase in SSP in binders decreased the slump flow, T500, and T700, and as per the fresh properties requirement, the optimum percentage of SSP that can be used in HSC is 5%.
- WGP can also be utilized as fine aggregate that substantially reduces the consumption of natural sand. The increment of WGP as a fine aggregate reduced the flow properties, and the optimum percentage replacement of 5% WGP may be utilized in HSC.
- A maximum compressive strength of 112.91 MPa was found for the C75SSP5 mix at 56 days. The impact of increased SSP within binders enhanced compressive strength significantly, but 5% SSP and 5% WGP exhibited better compressive strength. In addition, the C75SSP5 mix was steam cured for three days at 90 °C, and compressive strength was achieved at about 154 MPa. Similar observations were made regarding split tensile strength and the modulus of elasticity.
- SEM microscope images of HSC with SSP exhibited dense and compact structures. However, a small number of unreacted particles were still present; reacting with heat or steam-curing regimes can compact HSC further.
- EDS analysis of HSC with SSP displayed the presence of various gels such as CSH, CASH, CH, and CC, which contribute to HSC's mechanical properties. The Ca/Si ratios in the SSP-based paste decreased while the Si/Al ratios increased, contributing to the mechanical properties of the HSC mixes.
- XRD analysis of HSC with SSP showed the presence of quartz, CSH, and ettringite. The cross-bonding approach increased the effectiveness of OPC, SSP, SF, and FA, resulting in a more compact binder system that significantly improved the HSC's mechanical properties.

- The predicted equations of HSC with SSP and WGP for split tensile strength, flexural strength, and modulus of elasticity are shown in the relationship.

Author Contributions: Conceptualization, P.P.S.; methodology, P.P.S. and A.U.R.; validation, P.P.S. and A.U.R.; formal analysis, P.P.S.; investigation, P.P.S. and B.H.V.P.; resources, A.U.R.; data curation, P.P.S. and B.H.V.P.; writing—original draft preparation, P.P.S.; writing—review and editing, P.P.S., A.U.R. and M.V.K.; visualization, P.P.S.; supervision, A.U.R.; project administration, P.P.S. and A.U.R. All authors have read and agreed to the published version of the manuscript.

Funding: This research received no external funding.

Data Availability Statement: All data analyzed during this study are included in this published article.

Acknowledgments: The authors are thankful to the Department of Civil Engineering, Manipal Institute of Technology, Manipal Academy of Higher Education, Manipal, Karnataka, India. The authors would also like to acknowledge the use of XRD and SEM–EDS at the central institute facility, Manipal Institute of Technology, Manipal Academy of Higher Education.

Conflicts of Interest: The authors declare that they have no known competing financial interests or personal relationships that could have appeared to influence the work reported in this paper. The authors declare no conflict of interest.

References

- Jagadisha, A.; Rao, K.B.; Nayak, G.; Kamath, M. Influence of nano-silica on the microstructural and mechanical properties of high-performance concrete of containing EAF aggregate and processed quarry dust. *Constr. Build. Mater.* **2021**, *304*, 124392. [[CrossRef](#)]
- De Matos, P.R.; Foiato, M.; Prudêncio, L.R., Jr. Ecological, fresh state and long-term mechanical properties of high-volume fly ash high-performance self-compacting concrete. *Constr. Build. Mater.* **2019**, *203*, 282–293. [[CrossRef](#)]
- Tantri, A.; Shenoy, A.; Nayak, G. Characterization of rheological and mechanical properties of self-compacting concrete with Indian standard gradation and particle packing gradations. In *Recent Trends in Civil Engineering*; Springer: Singapore, 2021; pp. 79–92. [[CrossRef](#)]
- Tantri, A.; Nayak, G.; Shenoy, A.; Shetty, K.K. Development of self-compacting concrete using Bailey aggregate grading technique in comparison with Indian standard code of practice. *J. Eng. Des. Technol.* **2021**, *20*, 1664–1697. [[CrossRef](#)]
- Alharbi, Y.R.; Abadel, A.A.; Salah, A.A.; Mayhoub, O.A.; Kohail, M. Engineering properties of alkali activated materials reactive powder concrete. *Constr. Build. Mater.* **2020**, *271*, 121550. [[CrossRef](#)]
- Paris, J.M.; Roessler, J.G.; Ferraro, C.C.; DeFord, H.D.; Townsend, T.G. A review of waste products utilized as supplements to Portland cement in concrete. *J. Clean. Prod.* **2016**, *121*, 1–18. [[CrossRef](#)]
- Khan, M.I. Evaluation of non-destructive testing of high strength concrete incorporating supplementary cementitious composites. *Resour. Conserv. Recycl.* **2012**, *61*, 125–129. [[CrossRef](#)]
- Oh, B.H.; Cha, S.W.; Jang, B.S.; Jang, S.Y. Development of high-performance concrete having high resistance to chloride penetration. *Nucl. Eng. Des.* **2002**, *212*, 221–231. [[CrossRef](#)]
- Shi, C.; Jiao, D.; Zhang, J.; Wang, D.; Zhang, Y.; Farzadnia, N.; Hu, X. Design of high performance concrete with multiple performance requirements for #2 Dongting Lake Bridge. *Constr. Build. Mater.* **2018**, *165*, 825–832. [[CrossRef](#)]
- Aitcin, P. The durability characteristics of high performance concrete: A review. *Cem. Concr. Compos.* **2003**, *25*, 409–420. [[CrossRef](#)]
- Luo, X.; Sun, W.; Nin Chan, S.Y. Effect of heating and cooling regimes on residual strength and microstructure of normal strength and high-performance concrete. *Cem. Concr. Res.* **2000**, *30*, 379–383. [[CrossRef](#)]
- An, M.; Huang, H.; Wang, Y.; Zhao, G. Effect of thermal cycling on the properties of high-performance concrete: Microstructure and mechanism. *Constr. Build. Mater.* **2020**, *243*, 118310. [[CrossRef](#)]
- Li, L.; Dabarera, A.G.; Dao, V. Time-zero and deformational characteristics of high performance concrete with and without superabsorbent polymers at early ages. *Constr. Build. Mater.* **2020**, *264*, 120262. [[CrossRef](#)]
- Shen, D.; Liu, X.; Zeng, X.; Zhao, X.; Jiang, G. Effect of polypropylene plastic fibers length on cracking resistance of high performance concrete at early age. *Constr. Build. Mater.* **2020**, *244*, 117874. [[CrossRef](#)]
- Kamath, M.; Prashant, S.; Kumar, M. Micro-characterisation of alkali activated paste with fly ash-GGBS-metakaolin binder system with ambient setting characteristics. *Constr. Build. Mater.* **2021**, *277*, 122323. [[CrossRef](#)]
- Kumar, M.; Shreelaxmi, P.; Kamath, M. Review on characteristics of sewage sludge ash and its partial replacement as binder material in concrete. In *Recent Trends in Civil Engineering: Select Proceedings of TMSF 2019*; Springer Nature: Cham, Switzerland, 2021; pp. 65–78. [[CrossRef](#)]
- Kamath, M.V.; Prashanth, S.; Kumar, M. Review of low to high strength alkali-activated and geopolymer concrete. In *Recent Trends in Civil Engineering*; Springer: Singapore, 2021; pp. 105–113. [[CrossRef](#)]

18. Kamath, M.V.; Prashanth, S.; Kumar, M.; Tantri, A. Machine-Learning-Algorithm to predict the High-Performance concrete compressive strength using multiple data. *J. Eng. Des. Technol.* **2022**. [[CrossRef](#)]
19. Abhishek, H.S.; Prashant, S.; Kamath, M.V.; Kumar, M. Fresh mechanical and durability properties of alkali-activated fly ash-slag concrete: A review. *Innov. Infrastruct. Solutions* **2021**, *7*, 116. [[CrossRef](#)]
20. Shoukry, H.; Perumal, P.; Abadel, A.; Alghamdi, H.; Alamri, M.; Abdel-Gawwad, H.A. Performance of limestone-calcined clay cement mortar incorporating high volume ferrochrome waste slag aggregate. *Constr. Build. Mater.* **2022**, *350*, 128928. [[CrossRef](#)]
21. Afroz, S.; Zhang, Y.; Nguyen, Q.D.; Kim, T.; Castel, A. Shrinkage of blended cement concrete with fly ash or limestone calcined clay. *Mater. Struct.* **2023**, *56*, 15. [[CrossRef](#)]
22. Rajan, H. S.; Kathirvel, P. Sustainable development of geopolymer binder using sodium silicate synthesized from agricultural waste. *J. Clean. Prod.* **2021**, *286*, 124959. [[CrossRef](#)]
23. Long, W.-J.; Wu, Z.; Khayat, K.H.; Wei, J.; Dong, B.; Xing, F.; Zhang, J. Design, dynamic performance and ecological efficiency of fiber-reinforced mortars with different binder systems: Ordinary Portland cement, limestone calcined clay cement and alkali-activated slag. *J. Clean. Prod.* **2022**, *337*, 130478. [[CrossRef](#)]
24. Mo, K.H.; Alengaram, U.J.; Jumaat, M.Z.; Lee, S.C.; Goh, W.I.; Yuen, C.W. Recycling of seashell waste in concrete: A review. *Constr. Build. Mater.* **2018**, *162*, 751–764. [[CrossRef](#)]
25. Pragadeesan, H. Effect on Strength Properties of Concrete Containing Seashell Powder as a Partial Substitution of Fine Aggregate and Silica Fume used as Admixture. *Int. J. Eng. Technol.* **2018**, *7*, 689–692. [[CrossRef](#)]
26. Liao, Y.; Shi, H.; Zhang, S.; Da, B.; Chen, D. Particle size effect of oyster shell on mortar: Experimental investigation and modeling. *Materials* **2021**, *14*, 6813. [[CrossRef](#)] [[PubMed](#)]
27. Seo, J.H.; Park, S.M.; Yang, B.J.; Jang, J.G. Calcined Oyster Shell Powder as an Expansive Additive in Cement Mortar. *Materials* **2019**, *12*, 1322. [[CrossRef](#)]
28. Torres-Quiroz, C.; Dissanayake, J.; Park, J. Oyster Shell Powder, Zeolite and Red Mud as Binders for Immobilising Toxic Metals in Fine Granular Contaminated Soils (from Industrial Zones in South Korea). *Int. J. Environ. Res. Public Health* **2021**, *18*, 2530. [[CrossRef](#)] [[PubMed](#)]
29. Aly, M.; Hashmi, M.; Olabi, A.; Messeiry, M.; Abadir, E.; Hussain, A. Effect of colloidal nano-silica on the mechanical and physical behaviour of waste-glass cement mortar. *Mater. Des.* **2012**, *33*, 127–135. [[CrossRef](#)]
30. Lin, K.-L.; Shiu, H.-S.; Shie, J.-L.; Cheng, T.-W.; Hwang, C.-L. Effect of composition on characteristics of thin film transistor liquid crystal display (TFT-LCD) waste glass-metakaolin-based geopolymers. *Constr. Build. Mater.* **2012**, *36*, 501–507. [[CrossRef](#)]
31. Steyn, Z.; Babafemi, A.; Fataar, H.; Combrinck, R. Concrete containing waste recycled glass, plastic and rubber as sand replacement. *Constr. Build. Mater.* **2020**, *269*, 121242. [[CrossRef](#)]
32. Shayan, A.; Xu, A. Value-added utilisation of waste glass in concrete. *Cem. Concr. Res.* **2004**, *34*, 81–89. [[CrossRef](#)]
33. Mehta, A.; Kar, D.; Ashish, K. Silica fume and waste glass in cement concrete production: A review. *J. Build. Eng.* **2020**, *29*, 100888. [[CrossRef](#)]
34. Pascual, A.B.; Tognonvi, T.M.; Tagnit-Hamou, A. Optimization study of waste glass powder-based alkali activated materials incorporating metakaolin: Activation and curing conditions. *J. Clean. Prod.* **2021**, *308*, 127435. [[CrossRef](#)]
35. Tho-In, T.; Sata, V.; Boonserm, K.; Chindaprasirt, P. Compressive strength and microstructure analysis of geopolymer paste using waste glass powder and fly ash. *J. Clean. Prod.* **2018**, *172*, 2892–2898. [[CrossRef](#)]
36. Tripathi, M.; Chauhan, V.B. Evaluation of waste glass powder to replace the clay in fired brick manufacturing as a construction material. *Innov. Infrastruct. Solut.* **2021**, *6*, 134. [[CrossRef](#)]
37. Matos, A.M.; Sousa-Coutinho, J. Durability of mortar using waste glass powder as cement replacement. *Constr. Build. Mater.* **2012**, *36*, 205–215. [[CrossRef](#)]
38. Alharbi, Y.R.; Aref, A.A. Engineering properties of high-volume fly ash modified cement incorporated with bottle glass waste nanoparticles. *Sustainability* **2022**, *14*, 12459. [[CrossRef](#)]
39. Zhang, Y.; Zhu, P.; Liao, Z.; Wang, L. Interfacial bond properties between normal strength concrete substrate and ultra-high performance concrete as a repair material. *Constr. Build. Mater.* **2020**, *235*, 117431. [[CrossRef](#)]
40. Shi, Y.; Long, G.; Ma, C.; Xie, Y.; He, J. Design and preparation of ultra-high performance concrete with low environmental impact. *J. Clean. Prod.* **2019**, *214*, 633–643. [[CrossRef](#)]
41. Xie, T.; Fang, C.; Ali, M.M.; Visintin, P. Characterizations of autogenous and drying shrinkage of ultra-high performance concrete (UHPC): An experimental study. *Cem. Concr. Compos.* **2018**, *91*, 156–173. [[CrossRef](#)]
42. Sadrmomtazi, A.; Tajasosi, S.; Tahmouresi, B. Effect of materials proportion on rheology and mechanical strength and microstructure of ultra-high performance concrete (UHPC). *Constr. Build. Mater.* **2018**, *187*, 1103–1112. [[CrossRef](#)]
43. Gökçe, H.S.; Sürmelioglu, S.; Andiç-Çakir, Ö. A new approach for production of reactive powder concrete: Lightweight reactive powder concrete (LRPC). *Mater. Struct.* **2016**, *50*, 1–9. [[CrossRef](#)]
44. Lee, C.H.; Lee, D.K.; Ali, M.A.; Kim, P.J. Effects of oyster shell on soil chemical and biological properties and cabbage productivity as a liming materials. *Waste Manag.* **2008**, *28*, 2702–2708. [[CrossRef](#)]
45. Lertwattanaruk, P.; Makul, N.; Siripattarapavat, C. Utilization of ground waste seashells in cement mortars for masonry and plastering. *J. Environ. Manag.* **2012**, *111*, 133–141. [[CrossRef](#)] [[PubMed](#)]
46. Li, G.; Xu, X.; Chen, E.; Fan, J.; Xiong, G. Properties of cement-based bricks with oyster-shells ash. *J. Clean. Prod.* **2015**, *91*, 279–287. [[CrossRef](#)]

47. Cuadrado-Rica, H.; Sebaibi, N.; Boutouil, M.; Boudart, B. Properties of ordinary concretes incorporating crushed queen scallop shells. *Mater. Struct.* **2015**, *49*, 1805–1816. [[CrossRef](#)]
48. Hasnaoui, A.; Bourguiba, A.; El Mendili, Y.; Sebaibi, N.; Boutouil, M. A preliminary investigation of a novel mortar based on alkali-activated seashell waste powder. *Powder Technol.* **2021**, *389*, 471–481. [[CrossRef](#)]
49. Ahsan, M.H.; Siddique, M.S.; Farooq, S.H.; Usman, M.; Aleem, M.A.U.; Hussain, M.; Hanif, A. Mechanical behavior of high-strength concrete incorporating seashell powder at elevated temperatures. *J. Build. Eng.* **2022**, *50*, 104226. [[CrossRef](#)]
50. Sangeetha, P.; Shanmugapriya, M.; Saravanan, K.S.; Prabhakaran, P.; Shashankar, V. Mechanical properties of concrete with seashell waste as partial replacement of cement and aggregate. *Mater. Today Proc.* **2021**, *61*, 320–326. [[CrossRef](#)]
51. Zhang, Y.; Wu, B.; Wang, J.; Liu, M.; Zhang, X. Reactive Powder Concrete Mix Ratio and Steel Fiber Content Optimization under Different Curing Conditions. *Materials* **2019**, *12*, 3615. [[CrossRef](#)]
52. Amin, M.; Abu El-Hassan, K. Effect of using different types of nano materials on mechanical properties of high strength concrete. *Constr. Build. Mater.* **2015**, *80*, 116–124. [[CrossRef](#)]
53. Zhao, S.; Fan, J.; Sun, W. Utilization of iron ore tailings as fine aggregate in ultra-high performance concrete. *Constr. Build. Mater.* **2013**, *50*, 540–548. [[CrossRef](#)]
54. Abuodeh, O.R.; Abdalla, J.A.; Hawileh, R.A. Assessment of compressive strength of Ultra-high Performance Concrete using deep machine learning techniques. *Appl. Soft Comput.* **2020**, *95*, 106552. [[CrossRef](#)]
55. Abbas, S.; Nehdi, M.L.; Saleem, M.A. Ultra-High Performance Concrete: Mechanical Performance, Durability, Sustainability and Implementation Challenges. *Int. J. Concr. Struct. Mater.* **2016**, *10*, 271–295. [[CrossRef](#)]
56. Ramagiri, K.K.; Chauhan, D.R.; Gupta, S.; Kar, A.; Adak, D.; Mukherjee, A. High-temperature performance of ambient-cured alkali-activated binder concrete. *Innov. Infrastruct. Solutions* **2021**, *6*, 71. [[CrossRef](#)]
57. Malaikah, A. A Proposed Relationship for the Modulus of Elasticity of High Strength Concrete Using Local Materials in Riyadh. *J. King Saud Univ. Eng. Sci.* **2005**, *17*, 131–141. [[CrossRef](#)]
58. Al-Shamiri, A.K.; Kim, J.H.; Yuan, T.-F.; Yoon, Y.S. Modeling the compressive strength of high-strength concrete: An extreme learning approach. *Constr. Build. Mater.* **2019**, *208*, 204–219. [[CrossRef](#)]
59. Paul, S.C.; Šavija, B.; Babafemi, A.J. A comprehensive review on mechanical and durability properties of cement-based materials containing waste recycled glass. *J. Clean. Prod.* **2018**, *198*, 891–906. [[CrossRef](#)]
60. Salahuddin, H.; Qureshi, L.A.; Nawaz, A.; Raza, S.S. Effect of recycled fine aggregates on performance of Reactive Powder Concrete. *Constr. Build. Mater.* **2020**, *243*, 118223. [[CrossRef](#)]
61. Singh, R.; Nayak, D.; Pandey, A.; Kumar, R.; Kumar, V. Effects of recycled fine aggregates on properties of concrete containing natural or recycled coarse aggregates: A comparative study. *J. Build. Eng.* **2021**, *45*, 103442. [[CrossRef](#)]

Disclaimer/Publisher's Note: The statements, opinions and data contained in all publications are solely those of the individual author(s) and contributor(s) and not of MDPI and/or the editor(s). MDPI and/or the editor(s) disclaim responsibility for any injury to people or property resulting from any ideas, methods, instructions or products referred to in the content.